To characterize the distortion of dynamic pressure in the plane of the leading screen, another parameter, Δq (in percent), was evaluated as follows:

$$\Delta q = \left(\frac{q_{\max} - q_{\min}}{q_{\text{avg}}}\right) \times 100 \qquad (17)$$

where the leading screen is considered to be the screen closest to the inlet plane. Figure 3 shows the effect of screen placement on test section flow quality, where x_1 is the leading screen location normalized by the inlet length. This figure illustrates the improved test section flow quality with placement of turbulence-management devices further upstream of the inlet, in a flow regime of lowered inlet-induced dynamic pressure distortions.

Conclusions

A method to predict two-dimensional subsonic wind tunnel inlet flowfields based on elliptic grid generation has been developed. This method can predict the inlet and test section velocity and total pressure fields routinely for inlets containing turbulence screens. Existing elliptic grid generation codes could be readily modified to attain this capability by evaluating the source term to model the effect of the turbulence screens on the total head distribution.

References

[1]Coirier, W.J., "A Computational Method for the Analysis of Low Speed Wind Tunnel Inlets with Screens Using an Application of Elliptic Grid Generation," Master's Thesis, Dept. of Aeronautical and Astronautical Engineering, Ohio State University, Columbus, March 1985.

[2]Wieghardt, K.E.G., "On the Resistance of Screens," *The Aeronautical Quarterly*, Vol. 17, 1953, pp. 186–192.

[3]DeVahl, D.G., "The Flow of Air Through Wire Screens," *Hydraulics and Fluid Mechnaics*, Pergamon, New York, 1964, pp. 191–192.

[4]Thomson, J.F., Warsi, Z.U.A., and Mastin, C.W., *Numerical Grid Generation: Foundations and Applications*," North Holland, New York, 1985.

Turbulence Structure in Microburst Phenomena

George Treviño*
Michigan Technological University, Houghton, Michigan

Nomenclature

$A_{ij}(r,t)$	= anisotropic tensor
$C_{ij}(r,t)$	= velocity-correlation tensor
$I_{ij}(r,t)$	= isotropic tensor
L	= correlation length of anisotropic turbulence
M	= mean-flow gradient
$S_{ijl}(r,t)$	= turbulence self-interaction tensor
U_i	= fluid velocity
$\bar{U}_i$	= mean-flow velocity
u_i	= turbulence velocity
$f(r,t)$	= longitudinal correlation function of isotropic turbulence
$g(r,t)$	= transverse correlation function of isotropic turbulence
$k(r,t)$	= arbitrary function of isotropic turbulence self-interaction tensor
σ	= turbulence intensity
Λ	= isotropic integral scale
$\Delta\Lambda$	= change in integral scale due to anisotropy

Introduction

IT is rapidly becoming evident that knowledge of the interplay between turbulence and the underlying mean wind is a major key to the understanding of the microburst phenomenon[1]; particularly if the attendant hazards to airplane safety and performance are to be faithfully simulated in a regulated laboratory environment.[2] Such simulations are of cardinal importance in control-motivated pilot training.[3] The question of how isotropic turbulence "scales" in a windshear is of primary interest, and its study duly constitutes the essence of the fundamental problem of the microburst-turbulence phenomenon. Fortunately, the equation which governs the relation between mean-wind and turbulence is well known and understood—it is the Navier-Stokes equation of hydrodynamics, and for a steady-state turbulent fluid is written as

$$\frac{\partial U_i U_l}{\partial x_l} \simeq \nu \frac{\partial^2 U_i}{\partial x_l \partial x_l}$$

Here U_i is the total flow, decomposing as $U_i = \bar{U}_i + u_i$, and pressure-forces have been neglected. Typically this equation is supplemented by the conservation of mass condition, $\partial U_i/\partial x_i = 0$, which also decomposes as $\partial \bar{U}_i/\partial x_i = 0$ and $\partial u_i/\partial x_i = 0$.

In the present endeavor, the effect on turbulence of a variable mean wind along the flight path of an aircraft is modeled and analyzed (see Fig. 1). The depicted headwind-to-tailwind swing is not at all uncommon in a scenario where an aircraft encounters a microburst as it is attempting to land in a thunderstorm (see Fig. 2). The accompanying variability in the mean aerodynamic lift is well-documented; but the effect of the ever-present turbulence, since its statistical characteristics are still somewhat unresolved, is a question for continued research. The following attempts to address this issue.

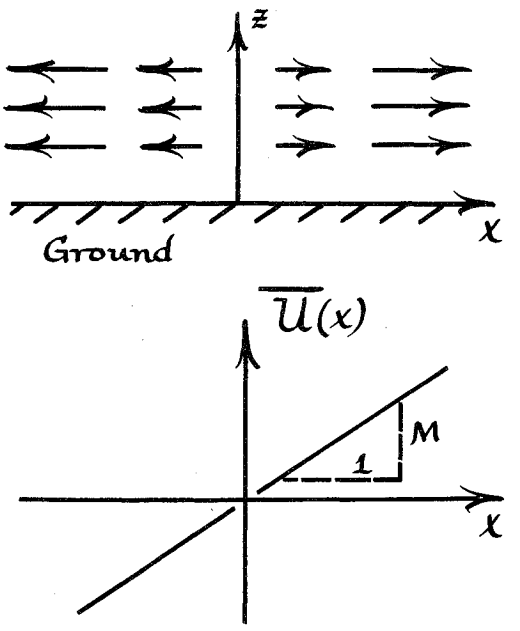

Fig. 1 Variable headwind or tailwind with velocity-gradient M.

Received Dec. 11, 1986.

*Associate Professor of Engineering Mechanics. Member AIAA.

Turbulence Characteristics

For the high Reynolds number case the attendant turbulence equation is

$$\frac{\partial \bar{U}_i}{\partial x_l} u_l + \bar{U}_l \frac{\partial u_i}{\partial x_l} + \frac{\partial (u_i u_l)}{\partial x_l} \simeq 0$$

here the operator, $[\bar{U}_l(\partial/\partial x_l)]$, automatically converts into $(\partial/\partial t)$, i.e., $\bar{U}_l\ (\partial/\partial x_l) \sim (\partial/\partial t)$, which means that as the airplane moves through the turbulence, any spatial changes in the turbulence structure (nonhomogeneities) are sensed as time-changes (nonstationarities) on the aircraft itself. Restricting the analysis to the two-dimensional case where $\bar{U} = (U(x), 0, W(z))$, and further $dU/dx = -dW/dz = M = a$ *positive constant,* the related two-point stochastic-averaged equation is

$$\frac{\partial}{\partial t} C_{ij}(r,t) + \frac{\partial \bar{U}_i}{\partial x} \langle u u_j' \rangle + \frac{\partial \bar{U}_i}{\partial z} \langle w u_j' \rangle + \frac{\partial \bar{U}_j}{\partial x'} \langle u' u_j \rangle + \frac{\partial \bar{U}_j'}{\partial z'} \langle w' u_i \rangle + \frac{\partial}{\partial r_l} S_{jli}(-r,t) - \frac{\partial}{\partial r_l} S_{ilj}(r,t) \simeq 0$$

where

$$\frac{\partial \bar{U}_i}{\partial x_l} = \frac{\partial \bar{U}_j'}{\partial x_l'} = \begin{vmatrix} M & 0 & 0 \\ 0 & 0 & 0 \\ 0 & 0 & -M \end{vmatrix}$$

The turbulence velocities are $u_i(x) = [u(x), 0, w(x)]$, and u_i' denotes $u_i(x') \equiv u_i(x+r)$. Later, when this equation is converted into a scalar equation, terms such as $(\partial \bar{U}_i/\partial x)\langle u u_j' \rangle$, will reduce to $(dU/dx)\langle u u' \rangle + (dW/dx)\langle u w' \rangle = M\langle u u' \rangle$.

Assuming that the turbulence is *anisotropic*, the tensor $C_{ij}(r,t)$ is expressed as $C_{ij}(r,t) = A r_i r_j + B\delta_{ij} + C\lambda_i\lambda_j + D(\lambda_i r_j + r_i \lambda_j)$, where $\lambda = (0,0,1)$ is a unit vector defining the vertical z direction as the preferred direction of the flow. However, along the airplane flight path (Fig. 2) the anisotropy is "small" and $C_{ij}(r,t)$ reduces[1] to $C_{ij}(r,t) \simeq A r_i r_j + B\delta_{ij} + C\lambda_i\lambda_j$, where $A = \sigma^2(f-g)/r^2$, $B = \sigma^2 g$, and $C = a|r| + b$; f and g are the longitudinal and transverse correlation functions of isotropic turbulence, respectively, while a and b are time-dependent parameters such that $a \sim 0(\alpha)$, $\alpha \sim$ glide-slope angle. This reduced version of $C_{ij}(r,t)$ can be used to derive the correspondingly reduced version of $S_{ijl}(r,t)$; accordingly,[4]

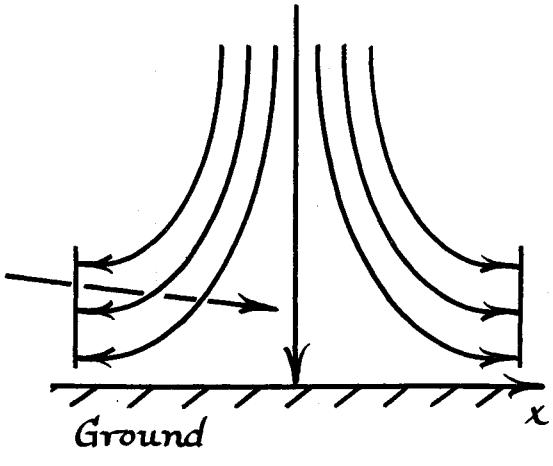

Fig. 2 Mean-velocity profiles for a turbulent microburst.

$$S_{ijl}(r,t) \sim \frac{\partial C_{ij}(r,t)}{\partial r_l} \to A r_i r_j r_l + B(r_i\delta_{jl} + r_j\delta_{il}) + C r_l \delta_{ij} + D r_l \lambda_i \lambda_j$$

where the conservation of mass constraint, $[\partial S_{ijl}(r,t)]/\partial r_l = 0$, imposes $D \equiv 0$. The form of the appropriate self-interaction tensor is therefore identical to that for isotropic turbulence; the importance of this result cannot be overemphasized.

Dynamical Consequences

The advantageous feature of the formulated anisotropy is that the tensor $C_{ij}(r,t)$ immediately separates into an isotropic part, say $I_{ij}(r,t)$, and an anisotropic part, say $A_{ij}(r,t)$; specifically, $C_{ij}(r,t) = I_{ij}(r,t) + A_{ij}(r,t)$, where $I_{ij}(r,t) = A r_i r_j + B\delta_{ij} \simeq \sigma^2\ [(f-g)/r^2] r_i r_j + \sigma^2 g \delta_{ij}$ and $A_{ij}(r,t) = C\lambda_i\lambda_j \simeq (a|r| + b)\lambda_i\lambda_j$. Dynamically, the problem also separates as

$$\frac{\partial I_{ij}(r,t)}{\partial t} + \frac{\partial}{\partial r_l} S_{jli}(-r,t) - \frac{\partial}{\partial r_l} S_{ilj}(r,t) \simeq 0$$

and

$$\frac{\partial A_{ij}(r,t)}{\partial t} + \frac{\partial \bar{U}_i}{\partial x} \langle u u_j' \rangle + \frac{\partial \bar{U}_i}{\partial z} \langle w u_j' \rangle + \frac{\partial \bar{U}_j'}{\partial x'} \langle u' u_i \rangle + \frac{\partial \bar{U}_j'}{\partial z'} \langle w' u_i \rangle \simeq 0$$

and solution of the isotropic part requires solution of the Karman-Howarth equation[5] for high Reynolds number turbulence, namely

$$\frac{\partial(\sigma^2 f)}{\partial t} \simeq \sigma^3 \left(\frac{\partial}{\partial r} + \frac{4}{r} \right) k$$

while solution of the anisotropic part requires solution of

$$\frac{\partial C}{\partial t} + 2M(\sigma^2(f-g) - (a|r| + b)) \simeq 0 \qquad (1)$$

A time-decay equation for the change $\Delta\Lambda$ in the isotropic integral scale Λ due to the modeled anisotropy is obtained by integrating Eq. (1) in r from $r=0$ to $r=\infty$. Accordingly, $[d(\sigma^2\Delta\Lambda)/dt] + M\sigma^2\Lambda - 2M\sigma^2\Delta\Lambda \simeq 0$, the solution of which is

$$\sigma^2\Delta\Lambda = -Me^{2Mt} \int e^{-2Mt} \sigma^2 \Lambda dt \qquad (2)$$

Recall[1] that $\int_0^\infty C dr \equiv \sigma^2\Delta\Lambda$, and $\Lambda = \int_0^\infty f dr$. Note that all factors in the integrand of Eq. (2) are positive, so that $\int e^{-2Mt} M\sigma^2\Lambda dt > 0$ for all t; furthermore, e^{+2Mt} is also positive so that $\sigma^2\Delta\Lambda = -$(positive number) < 0 for all relevant times. This means that the correlation length, $L = \Lambda + \Delta\Lambda$, which is sensed by the airplane as it moves through the microburst is always $L < \Lambda$, and the sensed turbulence is therefore *more random* than predicted by isotropy. Additionally, since $|\Delta\Lambda|$ increases with increasing time, the sensed turbulence becomes even more random as the aircraft continues to move through the microburst.

Concluding Remarks

It has been shown that the effect of a variable headwind or tailwind alters the magnitude of the length-scale of sensed microburst turbulence. The alteration has the effect of making the turbulence "more random" than what is ordinarily en-

countered in the upper atmosphere. This effect, coupled with the accompanying loss of aerodynamic lift unavoidably experienced in the headwind-to-tailwind swing, is what collectively creates the hazardous environment for an aircraft which encounters a microburst as it attempts to land in a thunderstorm.

Acknowledgments

This work was supported by NASA Langley through the American Society for Engineering Education Summer Faculty Research Program. The author enjoyed vigorous related discussions with Drs. R. L. Bowles, B. T. MacKissick, and K. Chuang, all of NASA Langley Research Center, and herewith acknowledges their collective participation in the completion of this work.

References

[1]Treviño, G., "Airplane Flight Through Wind-Shear Turbulence," *Journal of Aircraft*, Vol. 23, Sept. 1986, pp. 733–735.

[2]Chiles, J. R., "When Pilots' Worst Nightmares Come True—In Simulators," *Smithsonian*, June 1986, pp. 78–87.

[3]Treviño, G., "Turbulence for Flight Simulation," *Journal of Aircraft*, Vol. 23, April 1986, pp. 348–349.

[4]Robertson, H. P., "Invariant Theory of Isotropic Turbulence," *Proceedings of the Cambridge Philosophical Society*, Vol. 36, 1940, pp. 209–233.

[5]Batchelor, G. K., *Theory of Homogeneous Turbulence*, Cambridge University Press, Cambridge, England, 1967.

Propeller Swirl Effect on Single-Engine General-Aviation Aircraft Stall-Spin Tendencies

Joseph Katz*
San Diego State University, San Diego, California
and
Terry W. Feistel†
NASA Ames Research Center
Moffett Field, California

Introduction

THE considerable size and activity of the general-aviation fleet and its involvement in air accidents has focused attention on the safety of these aircraft. Among those accidents, the so-called "stall-spin" category accounted for more fatal and serious injuries than any other single type of accident.[1,2] The typical stall-spin occurs usually in low-airspeed maneuvers such as on final approach or following an engine failure. Because of the excessively low airspeed in these situations, the airplane operates close to its highest lift coefficient and any small lateral control input can result in a partial or full stall of one of the airplane's wings. Consequently, the stalled wing drops and creates larger drag which initiates the spinning motion of the airplane. On some aircraft, the stall-spin entry is so violent that most control surfaces are stalled and ineffective, and recovery is next to impossible with the available altitude. Therefore, estimating the propeller swirl effect on the lifting surfaces is critical since it introduces an asymmetric effect that is most pronounced in single-engine aircraft or in the "engine out" case of a twin-engine aircraft.

In this study, the effect of propeller slipstream on the stall pattern of a single-engine, untapered, low-wing aircraft was investigated. This asymmetric propeller influence can trigger an early stall of one of the wings and thereby can aggravate the spin-entry condition. Furthermore, it is shown that the combination of this propeller-induced effect with adverse sideslip can result in very large and abrupt changes in the rolling moment. This hazardous condition is likely to occur during uncoordinated, low-speed turning maneuvers, when the pilot yaws the aircraft to keep the wings level, instead of rolling it.

Discussion

Experimental development of stall-spin resistant general-aviation wings was sought by several research groups.[3-6] One of the methods investigated that showed partial success was to obtain gradual flow separation on both wings, thereby providing early stall warning as well as eliminating abrupt lift loss and violent changes in the rolling moment. The results reported here are the product of this effort, conducted at the NASA Ames 40×80 ft, full-scale wind tunnel.

The test airplane, as mounted in the wind tunnel is shown in Fig. 1. The airspeed was set to simulate the approach condition of about 124 km/h (77 mph), and the aircraft, piston-engine-driven propeller could be remotely operated. Further details on the experimental setup are reported by Feistel et al.[6]

The lift coefficient C_L and rolling moment coefficient C_R vs angle of attack α for the basic airplane with different power settings are shown in Fig. 2. The diamond symbols stand for the power-off data. The lift coefficient, in the lower section of the figure, shows fairly linear behavior up to an angle of attack of about 12 deg. In that region, the rolling moments are small and their scatter about the α axis is due to limited local separation at the wing's trailing edge (by the wing/fuselage junction). The triangular and circular symbols in Fig. 2 represent the data taken at 1800 and 2450 rpm, respectively, with flaps down ($\delta_f = 33$ deg). The case of 1800 rpm and flaps down corresponds to typical approach conditions, where stall-spin accidents are most likely to occur. The effect of flap deflection in the unseparated region of α is most pronounced on the lift curve (Fig. 2). The rolling-moment data, however, are almost unaffected, apart from a slight positive shift for the increased power setting.

The critical range of angle of attack for stall-spin alleviation for this particular aircraft is in the range of 10 deg $< \alpha <$ 16 deg, where the transition from attached to separated flow over the wing is developed. Figure 2 shows that through the stall region and beyond (10 deg $< \alpha <$ 16 deg), the rolling moment without the propeller effect is relatively small, whereas with increased power settings (constant pitch) the rolling moment increases violently in the negative direction. This is a result of the swirl caused by a clockwise propeller rotation (as seen from the pilot's point of view.) Therefore, because of the excess upwash at the left wing's root section, the flow over this wing separates first (at $\alpha \approx 13$ deg for 1800 rpm and $\alpha \approx 14$ deg for 2450 rpm), as shown by the inset of Fig. 2. Consequently, the negative rolling moment grows beyond control[6] (control limits are about $C_R \approx \pm 0.03$). After an additional increase of 3 deg in angle of attack, the right wing starts to stall, causing a reduction in the magnitude of the negative rolling moment. This process ended at about $\alpha \simeq 17$ deg with larger areas of flow separation on the right wing than on the left one. Flow visualizations (by tufts) verified this asymmetry of the stall pattern, which explains the second peak in the magnitude of the rolling moment (but this time to the positive direction).

Similar behavior of single-engine, low-wing aircraft was reported in Refs. 7–9. In Ref. 7, a large number of World War

Received Aug. 31, 1986; revision received Nov. 21, 1986.

*Professor, Department of Aerospace Engineering. Member AIAA.

†Aerospace Research Engineer, retired. Member AIAA.